The Finite Difference Method for *S*-Parameter Calculation of Arbitrary Three-Dimensional Structures

Steffen Haffa, *Member, IEEE,* Detlev Hollmann, *Member, IEEE,* and Werner Wiesbeck, *Senior Member, IEEE*

***Abstract*—This paper describes the application of the finite-difference method for the determination of scattering parameters of passive, arbitrary three-dimensional, lossy structures. Maxwell's equations are solved in the frequency domain by solution of a boundary value problem. The generalized *S*-parameters can be computed for any one port or two port structure, while, for the first time, dielectric and conductor losses are taken into account. Higher order mode coupling can be considered and different geometries are allowed at the input and output ports. Verification calculations are given and results are presented for typical structures.**

I. Introduction

An efficient design of monolithic integrated millimeter-wave circuits requires an exact knowledge of the electrical behavior of discontinuities and intersections. With increasing frequencies losses of the substrate and the metallization become more and more important and have to be considered. Therefore a powerful field theoretical method has to be applied instead of a time consuming trial and error procedure.

Several numerical methods have been presented in the literature but most of them are restricted to special geometries or they are not applicable due to lack of generality [1]–[8]. The spectral-domain approach is used in a wide field for computation of propagation characteristics of coupled lines [2]. However, it can only be applied to planar structures and losses are introduced by a perturbational calculation. Other procedures like the method of moments [3] require the knowledge of special functions as the Green's function, and are therefore mainly restricted to planar or symmetrical structures. A very flexible formulation is the finite-element method [4]–[6]. By using a triangular mesh a wide variety of geometries can be approximated, but the mesh generation is a major task. Suppression of spurious modes is another challenge which has to be accounted for.

A discretization of the differential Maxwell's equations in space and time is applied by the finite-difference time-domain method [9]–[14]. It has been used to perform time-domain simulations of pulse propagation in waveguide structures and microstrip circuits. Frequency-dependent scattering parameters can be calculated by Fourier transform of the time-domain results. Due to the fixed time step Δt the mesh has to be uniform. To accurately model sharp discontinuities a very small mesh size has to be employed, which leads to a very extensive computational effort.

The use of time-domain methods in the investigation of resonant structures requires small time steps to reach a sufficient resolution in the frequency domain. Because of the broad-band calculation any dispersive behavior of the material involved cannot be accounted for. The frequency-domain methods overcome these disadvantages by avoiding the Fourier transform and give the frequency dependent scattering parameters directly.

The finite-difference frequency-domain method has been successfully applied to eigenvalue problems for calculating the propagation characteristics of arbitrarily filled waveguides and resonant frequencies of cavity resonators [15], [16]. In our approach we present a more generalized version of a procedure, which has been introduced by Christ and Hartnagel [17], [18] to model MMIC chip interconnections.

After a description of the general formulation, including the discretization and the derivation of the scattering parameters, verifications are given for the numerical procedure. Example structures show the capabilities of the method and demonstrate the applicability to practical problems.

II. Computational Method

The structure under consideration is enclosed in a shielded rectangular box (Fig. 1). The whole box is divided into n elementary cells filled with arbitrary materials. Using this grid the three field components of the electric and magnetic fields are defined on every cell, which are used for discretization of Maxwell's equations. This leads to a relation between the field components of the neighboring cells. The combination of these relations give a linear system of equations. Its solution represents the complete electric field inside the whole structure. The

Manuscript received July 24, 1990; revised July 8, 1991.

S. Haffa and W. Wiesbeck are with the Institut fur Hochstfrequenztechnik und Electronik, University of Karlsruhe, 7500 Karlsruhe, Germany.

D. Hollmann is with Standard Elektrik Lorenz AG, 7530 Pforzheim, Germany.

IEEE Log Number 9104770.

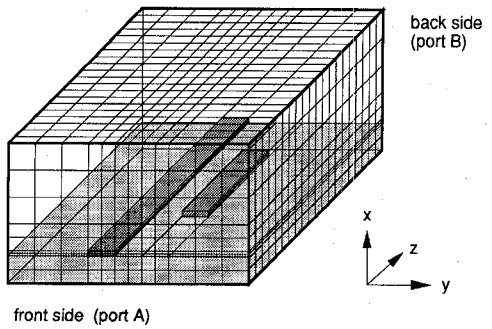

Fig. 1. Typical grid for a three-dimensional structure for discretization of Maxwell's equations and the coordinate system.

derivation of the equations is described in detail in Section II-A.

The walls of the box are perfectly conducting except for the two planes at the front and back sides. For *S*-parameter calculation the front and back sides of the structure are assumed to be connected to infinitely long transmission lines. The modal fields are given by the solution of the associated two dimensional eigenvalue problem on each port. In Section II-B the 2-D-problem is solved by the finite difference method for structures homogeneous in the direction of propagation.

Section II-C describes the procedure of *S*-parameter evaluation from the results of the three-dimensional field computations.

A. Discretization of the Field Equations

The grid used for discretization has been chosen to be nonequidistant Cartesian (Fig. 1) to simplify the mesh generation and to provide a sparse diagonal matrix of the resulting system of equations. The three space coordinates of the electrical field are defined upon an elementary cell of the grid. The actual cell is marked by the index k and has the dimensions x_k, y_k, and z_k as shown in Fig. 2(a). It consists of a material having a scalar complex permittivity and permeability. The electric field components E_k (Fig. 2(b)) are located on the middle of the edges and are assumed to be constant along the edge. Similarly a second grid is defined for the magnetic flux density B_k. Both grids are combined by placing the components of B_k at the center of each face of the E-mesh. This kind of allocation has the advantage that Maxwell's equations are always satisfied, even with different materials, because transition from one cell to the next involves continuous parallel E-field and perpendicular B-field components.

In the following $\vec{E}$ and $\vec{H}$ are the electric and magnetic field strengths, $\vec{D}$ and $\vec{B}$ the flux densities and $\vec{J}_e$ the source current density. All field components and material related parameters are allowed to be complex. With a harmonic time dependence of the form exp $(j\omega t)$, Maxwell's equations in integral form can be written:

$$\oint_C \vec{H} \cdot d\vec{s} = \int_A (j\omega\vec{D} + \kappa\vec{E}) \cdot d\vec{A} + \int_A \vec{J}_e \cdot d\vec{A} \tag{1a}$$

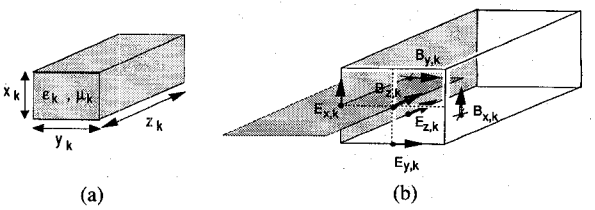

Fig. 2. Elementary cell k. (a) Dimensions and material. (b) Allocation of the electric and magnetic field components.

$$\oint_C \vec{E} \cdot d\vec{s} = -\int_A j\omega\vec{B} \cdot d\vec{A} \tag{1b}$$

$$\oint_A (j\omega\vec{D} + \kappa\vec{E}) \cdot d\vec{A} = 0 \tag{1c}$$

$$\oint_A \vec{B} \cdot d\vec{A} = 0 \tag{1d}$$

with the relations

$$\vec{D} = \epsilon\vec{E} \tag{1e}$$

$$\vec{B} = \mu\vec{H} \tag{1f}$$

where

ω	angular frequency
κ	conductivity
$\epsilon = \epsilon_0(\epsilon' - j\epsilon'')$	complex permittivity
$\mu = \mu_0(\mu' - j\mu'')$	complex permeability.

In this paper a source free structure is assumed ($\vec{J}_e = 0$). Dielectric losses (tan δ) have been taken into account by the complex permittivity ϵ. The finite conductivity κ is included in the frequency dependent imaginary part of the permittivity—see (2). This leads to a new complex dielectric constant $\epsilon^* = \epsilon_0 \cdot \epsilon_k$. In the following the complex material parameter ϵ_k of the cell k will be used. The values ϵ_k are complex in general, but real for lossless structures:

$$\Rightarrow \epsilon^* = \epsilon_0 \cdot \epsilon_k = \epsilon_0\left[\epsilon' - j\left(\epsilon' \tan\delta + 120\,\pi\Omega\,\frac{\kappa}{k_0}\right)\right]$$

$$k_0 = \omega \cdot \sqrt{\epsilon_0\mu_0} \quad \text{wave number.} \tag{2}$$

Maxwell's first and second equation, (1a) and (1b), respectively, can be discretized for every cell by a lowest-order integration formula. The integration planes for the elementary cell k are shaded in Fig. 2(b). Along the integration path field components of the neighboring cells are required. According to Fig. 3 indices are assigned to these cells in the following way: the actual cell is named k and the neighboring cells in y-direction are named l and r (left, right), whereas the cells in x-direction are marked by u and a (under, above). The letters f and b are used for the cells located in the planes in front (f) and behind (b) the actual plane. Combinations of these are used to mark

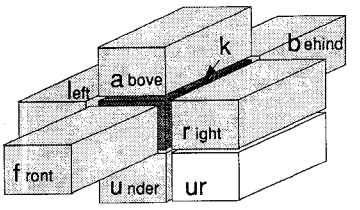

Fig. 3. Indexing scheme for the neighboring cells.

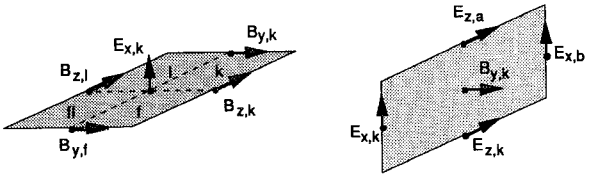

(a) (b)

Fig. 4. Integration planes for discretization of first and second of Maxwells' equation. (a) Equation (1a). (b) Equation (1b).

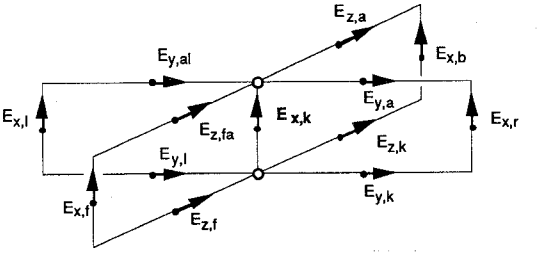

Fig. 5. E components, which correspond to the $E_{x,k}$ component in the three-dimensional case.

further surrounding cells. Equation (1b) leads to (see Fig. 4(b))

$$x_k E_{x,b} - z_k E_{z,a} - x_k E_{x,k} + z_k E_{z,k} = -j\omega z_k x_k B_{y,k}. \quad (3)$$

Similarly, (1a) can be written as (4) according to Fig. 4(a), noticing that the integration plane is divided into four rectangles which may consist of different materials (cells k, l, f and fl). For simplification some abbreviations, introduced in (5), define an equivalent length s_k and an equivalent area F_k:

$$s_{z,k}H_{z,k} - s_{y,k}H_{y,k} - s_{z,l}H_{z,l} + s_{y,f}H_{y,f} = \frac{j\omega\epsilon_0}{4} \cdot F_{x,k} \cdot E_{x,k} \quad (4)$$

$$s_{z,k}H_{z,k} = \frac{1}{2\mu_0}\left(\frac{z_f}{\mu_f} + \frac{z_k}{\mu_k}\right)B_{z,k} \quad (5a)$$

$$F_{x,k} = y_k z_k \epsilon_k + y_l z_k \epsilon_l + y_l z_f \epsilon_{fl} + y_k z_f \epsilon_f. \quad (5b)$$

Two similar equations can be deduced for the y and z components of the E-field. Setting up (3) for all B-components, which are involved in (4), and combining them allows elimination of the B-fields. This leads to (6) for the x-component of the electrical field $E_{x,k}$:

$$\begin{aligned}&\frac{s_{z,k}}{x_k}E_{y,a} - \frac{s_{z,k}}{y_k}E_{x,r} - \frac{s_{z,k}}{x_k}E_{y,k} - \frac{s_{y,k}}{z_k}E_{x,b}\\ &+ \frac{s_{y,k}}{x_k}E_{z,a} - \frac{s_{y,k}}{x_k}E_{z,k} - \frac{s_{z,l}}{x_l}E_{y,al} + \frac{s_{z,l}}{x_l}E_{y,l}\\ &- \frac{s_{z,l}}{y_l}E_{x,l} - \frac{s_{y,f}}{x_f}E_{z,af} - \frac{s_{y,f}}{z_f}E_{x,f} + \frac{s_{y,f}}{x_f}E_{z,f}\\ &+ \left(\frac{s_{z,k}}{y_k} + \frac{s_{y,k}}{z_k} + \frac{s_{z,l}}{y_l} + \frac{s_{y,f}}{z_f} - k_0^2 \cdot F_{x,k}\right)\\ &\cdot E_{x,k} = 0 \end{aligned} \quad (6)$$

Fig. 5 shows the 12 field components, which define the E-field component in x-direction of cell k. Similar equations can be set up for the $E_{y,k}$ and $E_{z,k}$ components. Up to now equations have been derived which define a relation between the E-field of cell k and the neighboring cells. Doing this for all n cells of the whole structure results in a linear system of equations which is written as

$$[C]\vec{E} = \vec{E}_r. \quad (7)$$

The matrix $[C]$ contains the geometry and the material parameters of the three-dimensional problem (the factors in (6)). $\vec{E}_r$ in (7), represents the exciting fields at the input and output ports (front and back side in Fig. 1). If they are set zero (electric wall) an eigenvalue problem is defined. For S-parameter evaluation however, the front and back side, called port A and B of the structure, are connected to two transmission lines of infinite lengths. The electric fields at those ports have to be the eigenvectors of the resulting 2-D structure. Their computation is described in the next section.

In the case of a lossless structure it can be shown that the resulting system of equations reduces to a real one. Equation (7) contains the E_x, E_y and the E_z components for all n nodes, thus the matrix is of order $3n \cdot 3n$. Due to the rectangular grid, the matrix $[C]$ is sparse with only 25 diagonals.

If losses are incorporated or if wave propagation along the structure is simulated to study interactions of discontinuities, all field components will be complex. The complex system of equations (7) must be changed to a real system, because the most efficient numerical equation solvers only deal with real matrices (i.e., [22]). To take advantage of this, (7) is splitted in its real (RE) and imaginary (IM) part. This leads to a $6n$ by $6n$ matrix, which is real. Equation (8) shows the six rows of the system for one node.

$$\begin{bmatrix} \ddots & \ddots & \ddots \\ \ddots & \ddots & \ddots \\ \ddots & \ddots & \ddots \end{bmatrix}_C \cdot \begin{vmatrix} \vdots \\ E^{RE}_{x,k} \\ E^{IM}_{x,k} \\ E^{RE}_{y,k} \\ E^{IM}_{y,k} \\ E^{RE}_{z,k} \\ E^{IM}_{z,k} \\ \vdots \end{vmatrix} = \begin{vmatrix} \vdots \\ E^{RE}_{xr,k} \\ E^{IM}_{xr,k} \\ E^{RE}_{yr,k} \\ E^{IM}_{yr,k} \\ E^{RE}_{zr,k} \\ E^{IM}_{zr,k} \\ \vdots \end{vmatrix}. \quad (8)$$

If the node is at the interface ports A or B, the right side is not zero and contains the exciting field. The number of diagonals increases from 25 in the lossless case to 27 for dielectric and conductor losses, and to 57 for dielectric, magnetic and conductor losses.

The solution of the resulting system of equations is performed on a supercomputer, which allows to deal with up to 55 000 elementary cells. A routine, based on the biconjugate-gradient method is applied, which takes advantage of the numerical form of the matrix [22], [23]. After the solution is computed, the electric field in every cell is available, not only for S-parameter calculation, but also to give insight into the electrical behavior and interactions of the structure. This can be demonstrated by three-dimensional graphical representation of the distribution of H-field and power flux density.

B. Two-Dimensional Analysis of the Field at the Ports

As previously mentioned, the structure under investigation is connected to infinitely long transmission lines at both ports, which are homogeneous in z direction. Thus the problem of determining the field distribution of the propagation modes reduces to a two-dimensional one.

The discretization procedure for Maxwell's equations is the same as in the three-dimensional case, but it simplifies because the dependency of the field components in z-direction is known. The fields at the plane in front (f) and behind (b) (Fig. 3) at a distance of Δz are related to the fields of the actual plane k by the propagation constant k_z of the considered mode:

$$E_{x,f} = E_{x,k}e^{+jk_z\Delta z};\quad E_{y,f} = E_{y,k}e^{+jk_z\Delta z};$$
$$E_{z,f} = E_{z,k}e^{+jk_z\Delta z} \tag{9a}$$

$$E_{x,b} = E_{x,k}e^{-jk_z\Delta z};\quad E_{y,b} = E_{y,k}e^{-jk_z\Delta z};$$
$$E_{z,b} = E_{z,k}e^{-jk_z\Delta z}. \tag{9b}$$

To eliminate the z-components of the electric field the discrete form of the continuity equation (1c) is applied. The values F_k are defined according to (5b):

$$F_{x,u}E_{x,u} - F_{x,k}E_{x,k} + F_{y,l}E_{y,l} - F_{y,k}E_{y,k} + F_{z,f}E_{z,f} - F_{z,k}E_{z,k} = 0 \tag{10}$$

If (6) and (10) are combined, and the field components of the plane in front ($E_{x,f}$, $E_{y,f}$, $E_{z,f}$) and behind ($E_{x,b}$, $E_{y,b}$, $E_{z,b}$) are expressed (9), an equation for the $E_{x,k}$ component at node k results. Thus, after some calculations an equation can be derived in terms of only E_x and E_y in one plane of the longitudinal homogeneous structure:

$$A_{k,1}E_{y,a} + A_{k,2}E_{x,r} + A_{k,3}E_{y,k} + A_{k,4}E_{y,al} + A_{k,5}E_{x,l} + A_{k,6}E_{y,l} + A_{k,7}E_{x,a} + A_{k,8}E_{x,u} + (A_{k,9} - (e^{-jk_z\Delta z} + e^{jk_z\Delta z}))E_{x,k} = 0. \tag{11}$$

Equation (11) is represented by Fig. 6. A similar relation can be deduced for the E-field in the y-direction $E_{y,k}$.

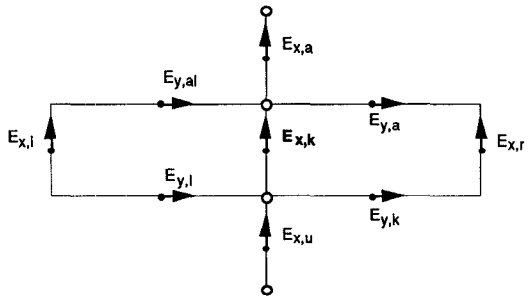

Fig. 6. $E_{x,k}$ and related E components for the two-dimensional solution with z homogeneity implied.

The coefficients $A_{k,i}$ are complex for any kind of losses in the structure. Setting up these equations for the x- and y-components of the electric field leads to an eigenvalue problem of the form

$$([A] - \gamma \cdot [I]) \cdot \vec{E} = \vec{0}$$
$$[I]\text{: unity matrix} \tag{12}$$

that is to be solved for γ. The eigenvalues γ are related to the complex propagation constant k_z by

$$k_z = -\frac{i}{\Delta z}\ln\left(\frac{\gamma}{2} + 1 - \sqrt{\frac{\gamma}{2}\left(\frac{\gamma}{2} + 2\right)}\right). \tag{13}$$

For an efficient computation only nonzero elements are included in the system, so the size of the matrix $[A]$ is $2m$, where m is the number of nonideal conducting cells in the z-plane.

A further drastical reduction of computation time can be achieved if the structure is symmetrical with respect to the x-z-plane, which is true in most practical cases. Then an electric or a magnetic wall can be defined in the middle of the structure. For the electric wall the Dirichlet boundary condition can be applied, that is, the tangential components E_t of the electric field must vanish at the wall. For the magnetic wall, the magnetic field is subject to the Neumann boundary condition, which can be rewritten as a condition for the electric field components perpendicular to the wall. Both conditions can be applied to (11) by eliminating the coefficients $A_{k,n}$ of the cells beyond the wall. The resulting matrix is reduced to half the size of the original matrix.

To get all numerical modes, the number of which is as high as the dimension of the matrix $[A]$, the calculations with the electric and the magnetic wall are combined. Using a magnetic wall for a first computation and an electric for the second, all available modes are computed for the whole grid structure. The results are merged to give the same result as after a computation without walls but with reduced computation time due to the smaller size of the matrix (half that of the computation without walls).

After the propagation constants have been computed for the desired modes, the transverse electric field (eigenvector) can be calculated for each mode as the solution of the homogeneous linear system of equations (12). This leads to m orthogonal eigenvectors. For normalization the or-

thogonality relation (14) is applied for each mode ($i = k$). The integration is performed across the two-dimensional structure. The E fields are normalized, so that the c_{ii} are real and equal to one. Additionally the orthogonality relation between different modes is tested to prove the accuracy of the field computation:

$$\int_A (\vec{E}_{ti} \times \vec{H}_{tk})\, \vec{dA} = c_{ik} \cdot \delta_{ik}. \tag{14}$$

For verification several two-dimensional structures have been investigated and the results have been checked against available analytical solutions. The results of a rectangular waveguide of height $= 5a$ and width $= 10a$, filled with lossy dielectric material are given in Table I. The propagation constant indicates a smooth transition at the cutoff between the normalized frequencies $ak_0 = 0.2$ and 0.3 due to the losses. The numerical result of the propagation constant is compared with the exact solution [19] and the resulting error is given in the last column. The table shows an error in real and imaginary part of less than 0.3% over the whole frequency range. The error increases near the cutoff due to the difference in the cutoff frequency of the physical mode and the grid mode. Comparable solutions [6], [20], obtained by the finite element method, show similar accuracy.

A field plot of the transverse modal field of the TM_{21} mode of the same waveguide is shown in Fig. 7. The electric and magnetic field lines show excellent agreement with [21], even for this mode of order seven. The tics on each side on the graph indicate the division of the mesh used for computation.

TABLE I
PROPAGATION CONSTANTS OF A LOSSY WAVEGUIDE ($\epsilon_r = 1.5$, $\tan\delta = 0.1$) FOR THE TE_{10} MODE VERSUS FREQUENCY AND DEVIATION FROM THE EXACT SOLUTION

Frequency ak_0	Relative Propagation Constant		Error Compared to Exact Solution [19]	
	$\mathrm{Re}\left\{\frac{k_z}{k_0}\right\}$	$\mathrm{Im}\left\{\frac{k_z}{k_0}\right\}$	Δ Re	Δ Im
0.1	0.0260	−2.8896	0.08%	−0.12%
0.2	0.0762	−0.9839	0.25%	−0.25%
0.3	0.6473	−0.1159	0.29%	−0.26%
0.4	0.9438	−0.0795	0.07%	0.07%
0.5	1.0541	−0.0795	0.04%	−0.03%
0.6	1.1095	−0.0676	0.02%	0.02%

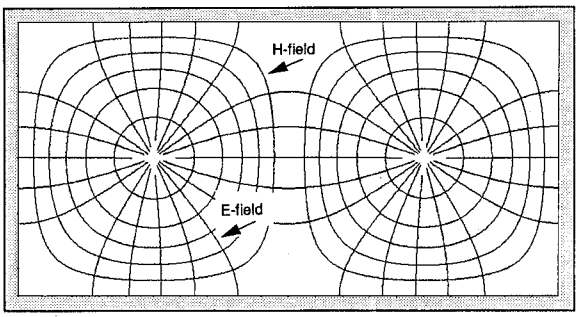

Fig. 7. E and H-field line plot of the TM_{21}-mode of a rectangular waveguide.

C. Determination of the Scattering Matrix

The method for evaluation of the scattering matrix is described extensively in [17], but for reason of completeness the main steps are presented in the following.

The ports at the three-dimensional structure under consideration are assumed to be connected to infinitely long transmission lines, whose modal fields have been computed by the 2-D eigenvalue problem as described above. Using these modal fields a generalized scattering matrix can be defined from the ratios of the emergent modes (b_i) and the incident modes (a_i) at both ports. Thus the scattering parameters define a relation between the different modes at each port and the transition behavior between both ports. The order of the matrix is $(k + l)$, where k is the number of modes at port A and l the number of modes at port B.

To compute the scattering matrix a linear superposition of the modal fields is applied at port A and B and the resulting electric field inside the structure is calculated. In every z-plane the tangential field $\vec{E}_t(z)$ can be splitted into the modal fields $\vec{E}_{ti}$, $\vec{H}_{ti}$ for mode i, using the orthogonality relation (15). Thus the contribution of the applied transverse electric field can be calculated at all z-planes inside the structure. It is now possible to determine the magnitude and phase of the two waves $a_i(z)$ and $b_i(z)$ for each mode i, propagating in $+z$ and $-z$-direction, by comparison of the values of the modal decomposition $w_i(z)$ at two neighboring z-planes:

$$\int_A (\vec{E}_t(z) \times \vec{H}_{ti})\, \vec{dA} = w_i(z) = a_i(z) + b_i(z). \tag{15}$$

Since the propagation characteristics of the mode amplitudes $a_i(z)$ and $b_i(z)$ are known at the input and the output ports, the reflection coefficients can be computed for the given field excitation. By combining a sufficient number $(k + l)$ of linear independent field excitations finally the generalized scattering parameters can be derived from the calculated reflection coefficients.

Higher order modes, excited at z-discontinuities, which are not considered at the ports, are treated to be ideally reflected at the connecting ports and may again interact with the propagating modes at the discontinuity. To avoid this, neglected modes must be attenuated sufficiently when they reach the input and output ports. Otherwise they have to be taken into account by including them into the modal superposition. Including more modes allows a shorter distance between the discontinuity and the input and output ports, thus the resulting matrix gets smaller. On the other hand the number of field excitations and the number of field computations depend on the number of considered modes. Therefore, to get small calculation times a tradeoff has to be found.

The accuracy of the scattering matrix elements can be

determined for any homogeneous transmission line. The reflection coefficients S_{11} and S_{22} have ideally to be zero. The parameters S_{21} and S_{12} can be compared to the transmission coefficients, derived from the propagation constant of the two-dimensional solution [24]. As an example a high loss microstrip transmission line of length $20a$ ($\tan\delta = 0.5$, $\kappa = 0.05$ Sm/mm^2) was investigated in the frequency range from $ak_0 = 0.02$ to $ak_0 = 0.2$. The calculated error of S_{12} and S_{21} is less 0.1 degree in phase and less 0.1% in magnitude. The reflection loss is better -60 dB. The errors of lossy structures agree very well to the estimations given in [18] for the lossless case.

III. Examples and Results

The following examples show the features of the method. They have been chosen to provide a comparison of these results to other methods e.g., achieved from two-dimensional formulations.

A microstrip line of 43 μm width with a metallization thickness of 3 μm, located on a 100 μm GaAs substrate, has been investigated. The electric field line plot (Fig. 8) shows the field concentrated beneath the conductor. Also some field lines end on the top of the microstrip line. A more impressive view can be given by the three-dimensional picture of the power flux density in z-direction (Fig. 9). The flux density $S_{z,z_0}(x, y)$ in z-direction in the plane $z = z_0$ has been calculated according (16) and is normalized to the power P_{z,z_0} divided by the area A of the cross-sectional plane $z = z_0$. This picture shows clearly the concentration of the power around the conductor of the microstrip line. The two peaks are located at the edges of the conductor. It can be seen that the microstrip mode is not disturbed by the enclosure:

$$P_{z,z_0} = \frac{1}{2}\,\mathrm{Re}\left\{\int_A (\vec{E}_t(x, y) \times \vec{H}_t^*(x, y))\, dA\right\} \tag{16a}$$

$$S_{z,z_0}(x, y) = \frac{A}{2P_{z,z_0}}\,\mathrm{Re}\,\{E_x H_y^* - E_y H_x^*\}. \tag{16b}$$

The scattering parameters of the three-dimensional calculation are related to the modal fields at both sides. However for CAD applications the characteristic impedance Z_L at the ports is required. Although the characteristic impedance is only defined for TEM modes, an equivalent value can be defined for quasi-TEM modes by using one of the following formulas:

$$Z_L^{(PU)} = \frac{|U_0|^2}{2P_z^*}, \quad U_0 = \int_a^b \vec{E}_t\, ds \tag{17a}$$

$$Z_L^{(PI)} = \frac{2P_z}{|I_{ZL}|^2}, \quad I_{ZL} = \oint \vec{H}_t\, ds \tag{17b}$$

$$Z_L^{(UI)} = \sqrt{Z_L^{(PI)} Z_L^{(PU)}} \tag{17c}$$

$$Z_L^{(\epsilon_{eff})} = \frac{Z_{L0}}{\sqrt{\epsilon_{\mathrm{eff}}}}. \tag{17d}$$

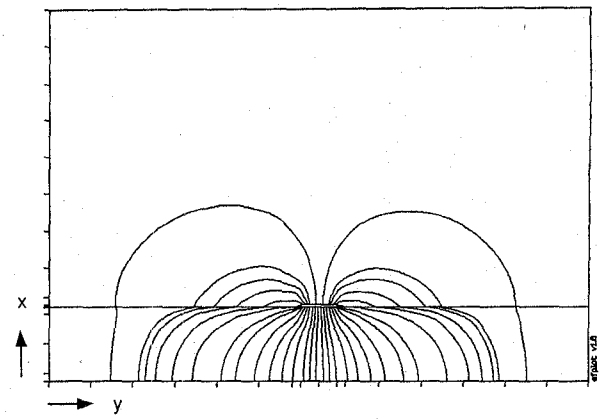

Fig. 8. Electric field distribution of a 43 μm microstrip line (metallization thickness = 3 μm) on 100 μm GaAs substrate ($\epsilon_r = 12.9$).

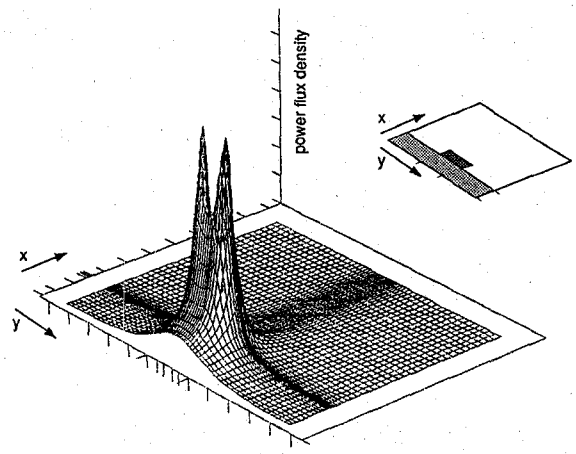

Fig. 9. Normalized power flux density on a microstrip in direction of propagation—same dimensions as in Fig. 9.

The line integral (17a) for the power voltage (PU) definition has to be performed from the inner conductor to the outer conductor, whereas the integration path of the loop integral (17b) (power current definition (PI)) has to enclose the microstrip line. The voltage current definition is either given by a direct calculation or by application of (17c). To apply definition (17d) the fields and propagation constants must be computed the same structure, but with all dielectrics replaced by air. This leads to the characteristic impedance in air Z_{L0}. In this case all three give the same result for Z_{L0}. For non-TEM modes the result depends on the integration path. Fig. 10 shows the calculated results for a microstrip transmission line versus frequency for the different definitions. For higher frequencies the values diverge due to the increasing concentration of the field under the microstrip, that means, the propagating mode loses its TEM behavior more and more. The results have been compared to a calculation using the spectral domain technique [2]. At low frequencies the values deviate by 5%. This correlates to a difference of 2.4% in the calculated voltage and current (17a), (17b). Our structure has a finite conductor thickness of 3 μm where the approach of [2] assumes a zero thickness. The same

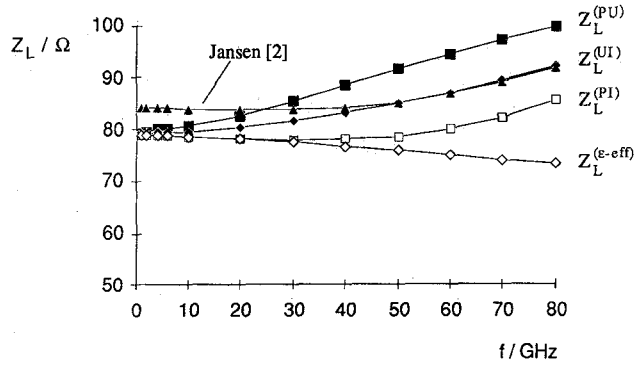

Fig. 10. Characteristic impedance Z_L of a microstrip (w = 30 μm, t = 3 μm, substrate: h = 200 μm, ϵ_r = 12.9) for various definitons.

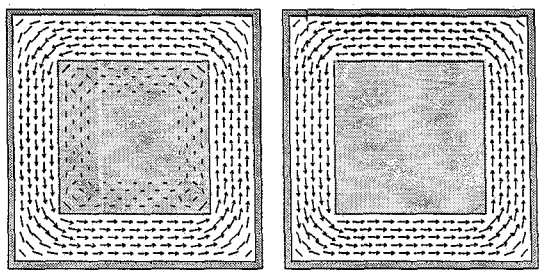

Fig. 11. Arrow field plot of a high lossy rectangular coaxial waveguide (inner conductor: $2a \times 2a$, width of outer conductor: $3.2a$, κ = 0.4 S · m/mm^2). (a) ak_0 = 0.01. (b) ak_0 = 0.3.

structure computed with conductor losses leads to a slight diminution of the real part of the impedances and to a negative imaginary part with an exponential decrease in magnitude versus frequency.

Conductor losses are included in the calculation by giving the conductors a finite value of κ. This may be demonstrated using a rectangular coaxial waveguide, with the inner conductor having a conductivity κ = 0.4 S · m/mm^2. At lower frequencies the H-field penetrates the lossy conductor, but at higher frequencies the conductor is free of field and the field concentrates in the surrounding region (Fig. 11).

A 43 μm microstrip line on GaAs substrate with a 50 μm gap is used to demonstrate the field distribution around the gap at about 50 GHz. The S-parameters demonstrate the behavior of the gap like a concentrated capacitor. A time dependent plot of the electric field is given in Fig. 12 in the intervals of 1/12 of the time period $T = 1/f$. The conditions for the electric field at the input and output ports have been chosen ideally matching. This has been achieved by a complex three-dimensional calculation with use of the previously computed scattering parameters. Thus a continuous wave propagation is ensured. A standing wave behavior in the region between the input port and the gap can be observed due to the reflections at the gap. The concentration of the field in the gap region can be studied.

A planar resistor of 50 Ω in series to a transmission line has been realized by a volume of resistive material. The

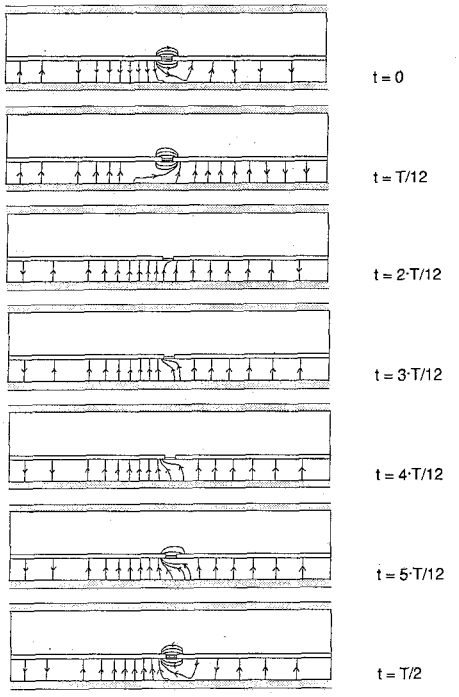

Fig. 12. Time dependence of the electric field beneath a microstrip line (conductor: width 43 μm, thickness 20 μm, substrate: height 100 μm, ϵ_r = 12.9) with a 50 μm gap.

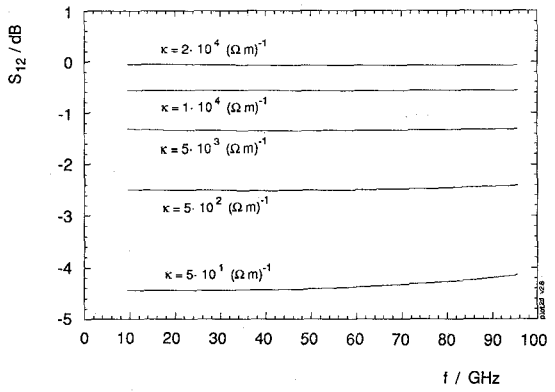

Fig. 13. Magnitude S_{12} of a planar series resistor at different conductivities κ (length 40 μm, width 43 μm, thickness 3 μm) in microstrip of same cross-section. Substrate: h = 150 μm, ϵ_r = 12.9.

magnitude of S_{12} (Fig. 13) shows a lumped element behavior over the whole frequency range. The structure can be represented by a series resistor, parallel to a capacitor. S_{12} increases with increasing frequency due to the capacitive coupling. The data in Fig. 13 are plotted after a shift of the reference plane to the ends of the resistor. The resulting values are in close agreement to a calculation of the dc values of the volume resistor (deviation $<$1% at 10 GHz).

An inductive post in a rectangular waveguide shows the validity of the method even for inhomogeneous three-dimensional structures. The wave incident upon the post is the dominant TE_{10} waveguide mode. The calculated scattering parameters are shown in Fig. 14 together with the results from Leviatan and Sheaffer [25]. Their solu-

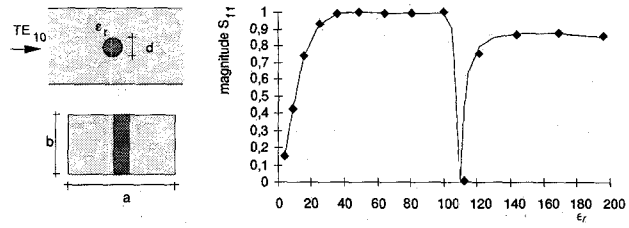

Fig. 14. Reflection coefficient magnitude S_{11} versus ϵ_r for a centered dielectric post in a rectangular waveguide ($b/a = 0.5$, $d/a = 0.1$, $a = \lambda/1.4$). The markers give the results from [25].

tion is based on a moment method, which uses filamentary currents to simulate the scattered field and the field inside the post. The agreement is very good even for high dielectric values of the post. The small shift of the resonance frequency is due to the slightly different post diameter resulting from the discretization.

VI. Conclusion

The presented method performs excellent results in *S*-parameter computation of discontinuity problems in planar transmission lines and even arbitrary three-dimensional structures. The finite-different method was formulated for analysis of three-dimensional lossy structures. The boundary conditions were chosen with precomputed electrical fields at the input and output port of the structure. Different excitations allow the evaluation of *S*-parameters of different modes, including coupling between higher order modes. The method was discussed in detail including the computation of the excited modal fields.

Numerical examples were given for various lossy and non lossy structures. Plots of the computed three-dimensional electric and magnetic fields provide informations on the behavior of the discontinuity. This will be of great use in the case of resonant or coupling structures, e.g., dielectric resonators coupled to a microstrip line. The use of a frequency-domain method allows the compution of scattering parameters with any necessary frequency resolution. Higher order modes excited by a discontinuity can be computed and the generalized *S*-parameters are used to describe the mode coupling. The achieved results are valid over a wide frequency range. The use of a supercomputer allows to treat large structures up to 55 000 elementary cells. The computing time depends on the structure and is up to a few minutes for each frequency point. The flexibility of this approach opens a wide variety of applications, i.e., monolithic microwave integrated circuits, waveguide transitions, electromagnetic compatibility, fields in biological media or similar structures.

References

[1] T. Itoh, Ed., *Numerical Techniques For Microwave and Millimeter-Wave Passive Structures*. New York: Wiley, 1989.

[2] R. H. Jansen, "The spectral-domain approach for microwave integrated circuits," *IEEE Trans. Microwave Theory Tech.*, vol. MTT-33, pp. 1043–1056, Oct. 1985.

[3] L. P. Dunleavy and P. B. Katehi, "A generalized method for analyzing shielded thin microstrip discontinuities," *IEEE Trans. Microwave Theory Tech.*, vol. 36, pp. 1758–1766, Dec. 1988.

[4] T. Angkaew, M. Matsuhara, and N. Kumagai, "Finite-element analysis of waveguide modes: A novel approach that eliminates spurious modes," *IEEE Trans. Microwave Theory Tech.*, vol. MTT-35, pp. 117–123, Feb. 1987.

[5] Z. Cendes, "Unlocking the magic of Maxwell's equations," *IEEE Spectrum*, vol. 26, pp. 29–33, Apr. 1989.

[6] J. Svedin, "A numerically efficient finite-element formulation for the general waveguide problem without spurious modes," *IEEE Trans. Microwave Theory Tech.*, vol. 37, pp. 1708–1715, Nov. 1989.

[7] S. Nam, H. Ling, and T. Itoh, "Characterization of uniform microstrip line and its discontinuities using the time-domain method of lines," *IEEE Trans. Microwave Theory Tech.*, vol. 37, pp. 2051–2057, Dec. 1989.

[8] P. So, Eswarappa, and W. Hoefer, "A two-dimensional transmission line matrix microwave field simulator using new concepts and procedures," *IEEE Trans. Microwave Theory Tech.*, vol. 37, pp. 1877–1884, Dec. 1989.

[9] K. S. Yee, "Numerical solution of initial boundary value problems involving Maxwell's equations in isotropic media," *IEEE Trans. Antennas Propagat.*, vol. AP-14, pp. 302–307, May 1966.

[10] A. Taflove and M. E. Brodwin, "Numerical solution of steady-state electromagnetic scattering problems using the time-dependent Maxwell's equations," *IEEE Trans. Microwave Theory Tech.*, vol. MTT-23, pp. 623–630, Aug. 1975.

[11] A. Taflove and K. Umashankar, "Radar cross section of general three-dimensional scatterers," *IEEE Trans. Electromagn. Compat.*, vol. EMC-25, pp. 433–440, Nov. 1983.

[12] D. H. Choi and W. Hoefer, "The finite-difference time-domain method and its application to eigenvalue problems," *IEEE Trans. Microwave Theory Tech.*, vol. MTT-34, pp. 1464–1469, Aug. 1986.

[13] G. C. Liang, Y. W. Liu, and K. K. Mei, "Full-wave analysis of coplanar waveguide and slotline using the time-domain finite-difference method," *IEEE Trans. Microwave Theory Tech.*, vol. 37, pp. 1949–1957, Dec. 1989.

[14] D. M. Sheen, S. M. Ali, M. D. Abouzahra, and J. A. Kong, "Application of the three-dimensional finite-difference time-domain method to the analysis of planar microstrip circuits," *IEEE Trans. Microwave Theory Tech.*, vol. 38, pp. 849–857, July 1990.

[15] T. Weiland, "On the numerical solution of Maxwellian eigenvalue problems in three dimensions," *Particle Accelerators*, vol. 17, pp. 227–242, 1985.

[16] ——, "Three-dimensional resonator mode computation by finite difference method," *IEEE Trans. Magn.*, vol. MAG-21, pp. 2340–2343, June 1984.

[17] A. Christ and H. Hartnagel, "Three-dimensional finite-difference method for the analysis of microwave-device embedding," *IEEE Trans. Microwave Theory Tech.*, vol. MTT-35, pp. 688–696, Aug. 1987.

[18] A. Christ, "Streumatrixberechnung mit dreidimensionalen Finite-Differenzen für Mikrowellen-Chip-Verbindungen und deren CAD-Modelle," Ph.D. dissertation, Fortschritt-Ber., VDI Reihe 21 Nr. 3, VDI Verlag Düsseldorf, 1988.

[19] R. E. Collin, *Field Theories of Guided Waves*. New York: McGraw Hill, 1960.

[20] K. Hayata *et al.*, "Finite-element formulation for lossy waveguides," *IEEE Trans. Microwave Theory Tech.*, vol. 36, pp. 117–123, Feb. 1988.

[21] N. Marcuvitz, *Waveguide Handbook, IEE Electromagnetic Waves Series*, vol. 21. London: Peregrinus Ltd., 1986.

[22] "LINSOL documentation," Computer Center Universität Karlsruhe.

[23] R. Fletcher, "Conjugate gradient methods for indefinite systems," *Lecture Notes in Mathematics, Numerical Analysis Dundee*. Berlin: Springer, pp, 73–89, 1975.

[24] D. Hollmann, S. Haffa, and W. Wiesbeck, "S-parameter calculation of arbitrary three-dimensional lossy structures by finite difference method," in *Proc. Int. Conf. on Directions in Electromagnetic Wave Modeling*, Weber Research Institute of Polytechnic University, New York, Oct. 1990.

[25] Y. Leviatan and G. S. Sheaffer, "Analysis of inductive dielectric posts in rectangular waveguide," *IEEE Trans. Microwave Theory Tech.*, vol. MTT-35, pp. 48–59, Jan. 1987.

Steffen Haffa (S'88–M'91) was born in Stuttgart, Germany, in 1956. He received the Dipl-Ing. (M.S.) degree from the University of Karlsruhe in 1983.

From 1983 to 1986 he was employed at Richard Hirschmann Company, Stuttgart. He was responsible for the development of satellite receiving systems, with the main work on reflector antennas and feed systems. Since 1986 he has been with the Institute for Microwaves and Electronics at the University Karlsruhe, where he received the Dr.-Ing. (Ph.D.) degree in 1990. His research work was on field theoretical computation for device modeling and measurement at mm-wave frequencies. The main application of his work was on GaAs MMIC.

Detlev Hollmann (S'88–M'91) was born in Karlsruhe, Germany, in 1960. He received the Dipl.-Ing. (M.S.) degree from the University of Karlsruhe in 1987.

He then joined the GaAs mm-wave group at the Standard Elektrik Lorenz AG (SEL), Pforzheim, where he is responsible for network measurement and calibration. In cooperation with the Institut for Microwaves and Electronics (IHE) at the University of Karlsruhe, he worked in the field of numerical computation of electromagnetic fields applied to dielectric resonator coupling on MMIC circuits and received the Dr.-Ing. (Ph.D.) degree in 1991. Currently, he is involved in the design of GaAs MMIC circuits for mm-wave communication systems.

Werner Wiesbeck (SM'87) was born near Munich, Germany in 1942. He received the Dipl.Ing. (M.E.E.) and the Dr.Ing. (Ph.D.E.E.) degrees from the Technical University Munich in 1969 and 1972, respectively.

From 1972 to 1983 he was with AEG-Telefunken in various positions including head of R&D of the Microwave Division in Flensburg and marketing director Receiver and Direction Finder Division Ulm. During this time he had product responsibility for mm-wave radars, receivers, direction finders and electronic warfare systems. Since 1983 he has been director of the Institute for Microwaves and Electronics at the University Karlsruhe. His present research topics include radar, remote sensing, wave propagation and antennas. In 1989 he spent a six month sabbatical at the Jet Propulsion Laboratory, Pasadena, CA.

Dr. Wiesbeck is engaged in several working groups in electrical engineering.